

Article

Corrosion of Metals and Nickel-Based Alloys in Liquid Bismuth–Lithium Alloy

Aleksandr V. Abramov ^{1,*}, Ruslan R. Alimgulov ², Anastasia I. Trubcheninova ², Arkadiy Yu. Zhilyakov ³, Sergey V. Belikov ³, Vladimir A. Volkovich ² and Ilya B. Polovov ²

¹ Department of Physical and Chemical Methods of Analysis, Ural Federal University, 620002 Ekaterinburg, Russia

² Department of Rare Metals and Nanomaterials, Ural Federal University, 620002 Ekaterinburg, Russia; aimgulovruslan@gmail.com (R.R.A.); atrubcheninova@gmail.com (A.I.T.); v.a.volkovich@urfu.ru (V.A.V.); i.b.polovov@urfu.ru (I.B.P.)

³ Department of Heat Treatment and Physics of Metals, Ural Federal University, 620002 Ekaterinburg, Russia; arkadiy_1989@mail.ru (A.Y.Z.); srgbelikov@yandex.ru (S.V.B.)

* Correspondence: abramov.urfu@mail.ru

Abstract: Bismuth–lithium alloys are considered as primary candidates for the reductive extraction step of on-line reprocessing of a molten salt reactor fuel. The corrosion behavior of pure metals and nickel-based alloys was studied in a liquid Bi–Li (5 mol.%) alloy at 650 °C. The tantalum, molybdenum, and corrosion-resistant alloys VDM[®] Alloy C-4, Hastelloy[®] G-35[®], KhN62M, VDM[®] Alloy 59 were studied as prospective materials for this liquid metal media. The corrosion rates were determined by gravimetric method as well as chemical analysis of corrosion products in Bi–Li alloy. Microstructure and chemical composition of samples of the materials and Bi–Li alloys containing the corrosion products after the tests were evaluated using inductively coupled plasma–atomic emission spectroscopy, X-ray fluorescence analysis, scanning electron microscopy, and energy dispersive spectroscopy. Metallic tantalum and molybdenum do not chemically interact with liquid Bi–Li alloy; the corrosion rate of these metals is determined only by the solubility in this medium. The corrosion rates of Ta and Mo at 650 °C were 0.09 and 0.07 mm/year, respectively. Nickel alloys are subjected to severe corrosion in liquid Bi–Li alloys due to dissolution of nickel in liquid bismuth. Alloys of this type cannot be used in such an environment.

Keywords: corrosion; bismuth; lithium; nickel alloys; tantalum; molybdenum



Citation: Abramov, A.V.; Alimgulov, R.R.; Trubcheninova, A.I.; Zhilyakov, A.Y.; Belikov, S.V.; Volkovich, V.A.; Polovov, I.B. Corrosion of Metals and Nickel-Based Alloys in Liquid Bismuth–Lithium Alloy. *Metals* **2021**, *11*, 791. <https://doi.org/10.3390/met11050791>

Academic Editor: Xing-Qiu Chen

Received: 17 March 2021

Accepted: 30 April 2021

Published: 13 May 2021

Publisher's Note: MDPI stays neutral with regard to jurisdictional claims in published maps and institutional affiliations.



Copyright: © 2021 by the authors. Licensee MDPI, Basel, Switzerland. This article is an open access article distributed under the terms and conditions of the Creative Commons Attribution (CC BY) license (<https://creativecommons.org/licenses/by/4.0/>).

1. Introduction

Liquid metals exhibit a number of properties, including high thermal and electric conductivity, fluidity, low volatility, and high boiling point, that make them attractive in various industrial applications, e.g., where efficient heat transfer is required. Low melting metals and their alloys with acceptable nuclear–physical characteristics (i.e., Li, Na, K, Pb, Bi) can be used as coolants in fast nuclear reactors [1,2], transport reactors for submarines [3], and reactors for space applications [4]. In addition, liquid metals can be used for reprocessing spent nuclear fuels (SNF) and, currently, a wide range of studies of promising methods of SNF reprocessing using liquid metal media [5] is under way.

However, the high corrosion rate of structural materials in liquid metals limits their widespread application [6]. The main cause of the corrosion processes in gases, aqueous solutions, and molten salts is the chemical or electrochemical interaction of materials with these media [7]. The primary cause of corrosion of materials in liquid metals and alloys is physical dissolution due to alloying processes. The rate of corrosion in liquid metal media depends on a number of factors, including dynamics (flow rate of the liquid metal relative to the solid material), temperature gradients in the system, and elemental and chemical composition of the structural materials and liquid metal media [8]. If liquid metals contain

impurities, then corrosion of materials can result from the redox reactions involving these impurities. In this case, physical dissolution of the structural materials can be very slow or even absent. Such processes were observed, for example, in molten alkali metals where the solubility of common metallic structural materials is low and the corrosion phenomena are mainly related to the reactions involving non-metallic impurities (carbon, hydrogen, nitrogen, oxygen) [9].

Corrosion of the materials (metals or alloys) can be uniform or localized along grain boundaries. If there is a noticeable difference in the solubility of alloy components, the metal with the highest solubility will be selectively etched from the solid, resulting in the formation of a surface zone depleted in this easily soluble element. This zone is termed the selective corrosion zone [8]. An example of such effect is the leaching nickel from austenitic chromium–nickel steels in molten lead, bismuth, and their alloys [10,11]. Localization of the corrosion process can lead to intercrystalline penetration of the liquid metal along the grain boundaries and subsequent embrittlement of the material [12]. Liquid metal embrittlement is a characteristic feature of typical ductile metals (Ni, Al, Cu). This phenomenon was studied in detail for binary systems containing a low melting metal, Ni–Bi, Cu–Bi, and Al–Ga [13,14]. Even low level of impurities (<0.5 at.% Fe, Sn, Mn) increased the penetration depth of liquid metal by a factor of 6 [15].

The majority of corrosion studies performed in liquid bismuth focused on various steels or individual metals, and the results are often contradictory. James and Trotman [16] reported that steels with high nickel and manganese content had very low corrosion resistance in liquid bismuth due to high solubility of Ni and Mn in Bi. The low-alloy steels exhibited higher corrosion resistance compared with the high-alloy steels. However, Horsley and Maskrey [17] demonstrated that the low-alloy steel of 2.25% Cr–1% Mo type had an extremely high corrosion rate in liquid bismuth under dynamic conditions (over 16.5 mm/year at 748–898 K and bismuth velocity of 3–4 mm/s). Dawe et al. [18] reported that the steel containing 12% chromium showed the lowest dissolution rate in liquid bismuth at temperatures to 823 K and no corrosion was detected after 2500 h. Similarly, Stephan and Koshuba [19] observed very low corrosion of a loop made of AISI 347 steel (containing 17–19% Cr and 9–13% Ni) after 100 h circulation of liquid bismuth at 900 °C. Additional studies are clearly needed to clarify the mechanisms of corrosion of metallic materials in liquid bismuth-based alloys.

The present work aimed to study the corrosion resistance of individual metals (Mo, Ta) and nickel-based alloys (Hastelloy® G-35®, VDM® Alloy C-4, KhN62M, VDM® Alloy 59) in a liquid Bi–Li alloy. During the reductive extraction step, the construction materials contact both liquid Bi–Li alloy and molten fluoride salt, and the choice of objects for the present study reflects this circumstance. Previously [20], we showed that molybdenum and nickel super alloys have high corrosion stability in fluoride melts; therefore, these metals were now selected for assessing their corrosion behavior in a Bi–Li alloy.

Past studies on the corrosion resistance of structural materials in contact with liquid metals showed that of all low melting metals commonly used as heat carriers (i.e., Li, Na, Pb, Bi), bismuth was the most corrosive [21]. Possible intermetallic compounds (IMCs) than can be formed by bismuth with the principal elements present in the structural materials are listed in Table 1 [22].

Table 1. Possible intermetallic compounds of metals with bismuth [22].

Element	Fe	Ni	Mo	W	Ta	Nb	Cr	Cu	Mn	Si	Zr
IMC	none	BiNi Bi ₃ Ni	none	none	none	none	none	none	MnBi	none	ZrBi ₂ ZrBi Zr ₃ Bi ₂ Zr ₃ Bi Zr ₃ Bi

Molybdenum and tantalum do not form IMCs with bismuth. The solubility of molybdenum in liquid bismuth does not exceed 10^{-4} wt.% at 1030 °C [23], and tantalum content in liquid bismuth after 120 h of contact at 778 °C was no more than 10^{-5} wt.% [24].

Nickel is the primary component of nickel-based alloys, and this element is capable of forming two intermetallic compounds with bismuth through peritectic reactions, BiNi (78.08 wt.% Bi) at 654 °C and Bi₃Ni (91.44 wt.% Bi) at 469 °C [23] (Table 1). However, when nickel was kept in contact with liquid bismuth for a long time these intermetallic compounds, initially formed on the surface, dissolved [25]. In the absence of stable IMCs between bismuth and tested structural materials, physical dissolution of the components would be the main mechanism of the corrosive action of liquid bismuth.

2. Materials and Methods

2.1. Materials

Samples of materials selected for the study were cut using a Discotom-6 (Struers) automatic cutting machine with water cooling of the cutting zone. Each sample of the alloy was sandpapered in five stages (SiC papers were used in the following order of grades: 80→220→320→1200→2400). The final surface roughness of the metallic samples (Ra) was below 0.4 mm. Each prepared billet was washed with water and rinsed in acetone. The samples were dried, weighed, and their surface area was measured. High-purity metals were used for this work (Mo > 99.95 wt.%, Ta > 99.9 wt.%). The metal samples were cylindrical, 10 mm high and 6 or 4 mm diameter for Mo and Ta, respectively. Samples of nickel-based alloys were cut from sheets 4–4.8 mm thick and were of a rectangular shape. The composition of the alloys in their as-received state is listed in Table 2. Metallic bismuth (KiteMetals) was of 99.99% purity. According to the manufacturer's specification the main impurities were Ag (0.0012 wt.%), Pb (0.0003 wt.%), As (0.0002 wt.%), and Cu, Fe, Sb, and Zn (0.0001 wt.% each). X-ray fluorescence analysis (XRF) of bismuth showed silver content of 0.0013 wt.%; all other impurities were below 0.001 wt.%. Lithium (99.9%) contained 0.01 wt.% Na, 0.03 wt.% Ca, 0.02 wt.% Mg, 0.005 wt.% K and Fe (according to the manufacturers' certificates).

Table 2. Composition of studied alloys according to the manufacturers' certificates, wt.%.

Alloy	Ni	Cr	Mo	Fe	Mn	Ti	Al	Si	S	C	P	Cu	W
VDM® Alloy C-4	base	16.1	15.6	0.84	0.02	0.01	—	0.016	0.002	0.003	0.002	—	—
Hastelloy® G-35®	base	33.12	8.22	0.78	0.22	<0.01	0.19	0.04	<0.002	0.012	0.003	0.03	0.11
KhN62M	base	23.21	12.78	0.47	0.03	0.08	0.11	0.06	0.003	0.005	0.004	—	—
VDM® Alloy 59	base	22.6	15.4	0.9	0.19	—	0.23	0.02	<0.002	0.002	0.002	<0.01	—

2.2. Corrosion Tests

The corrosion tests were carried out employing a custom-built setup for high-temperature corrosion studies as described in detail earlier [26]. This setup allows performing long-term corrosion tests in various working media at elevated temperatures. A stream of gas or a gas mixture can be constantly passed through the experimental cells if required. Corrosion experiments were performed in the following manner. Three samples of a selected metallic material were used in each test. The samples were placed in low-porosity graphite crucibles, metallic bismuth granules were loaded on top, then the required amount of lithium was added to achieve the molar ratio of lithium to bismuth of 1:19. Each crucible was placed in a steel cell that could be hermetically closed using steel lids. Metallic zirconium was placed on the bottom of the cell to act as a getter for purifying the atmosphere from oxygen impurities. The experimental setup used for the corrosion studies is schematically presented in Figure 1.

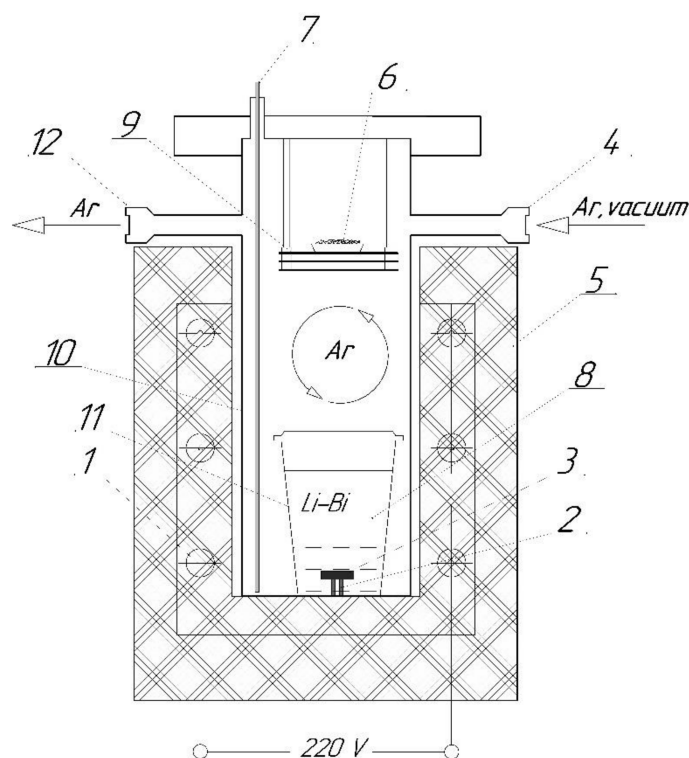


Figure 1. Experimental setup for corrosion experiments: heaters (1); sample holder (2); test sample (3); gas inlet (4); furnace (5); zirconium getter (6); thermocouple (7); liquid metal (8); nickel heat reflecting screens (9); steel cell (10); crucible (11); gas outlet (12).

Each cell was sealed, evacuated, filled with argon, and placed in a vertical tube furnace. A flow of high-purity argon (99.999%) through the cell was maintained for the duration of the experiments. Argon was passed through the upper part of the cell at ca. 50 mL/min flow rate. The duration of corrosion tests was 100 h. After completing the experiment, the cells were cooled to room temperature, opened, and the crucibles with the samples taken out. The samples were thoroughly washed and dried. After measuring weight loss, the specimens were mounted in phenol hot-mounting resin with carbon filler for metallographic analysis. Mounted samples were first sandpapered in six stages (SiC papers in the following order of grades: 80→220→320→1200→2400→4000). Finally, the samples were polished using water-based diamond suspension (monocrystalline diamonds with grain size of 1 μm , DiADuo-2, Struers) followed by colloidal silica polishing suspension (OP-S, Struers).

The surface of corroded samples was examined by scanning electron microscopy (SEM, JEOL JSM 6490) with energy dispersive X-ray microanalysis (EDS, Oxford Inca) and SEM (ThermoFisher Scios 2) with a microanalysis attachment (Inka Energy TEM 350).

Bismuth–lithium alloys (BLA) after the corrosion tests were analyzed by XRF (ARL Advant’X 4200) and inductively coupled plasma–atomic emission spectroscopy (ICP–AES, Optima 2100) to determine the content of impurities and the corrosion products.

3. Results and Discussion

The sample appearance prior to and after the corrosion tests in BLA is compared in Figure 2. Molybdenum and tantalum (c,d in Figure 2) show very little change while nickel-based alloys (a,b in Figure 2) have signs of severe corrosion.

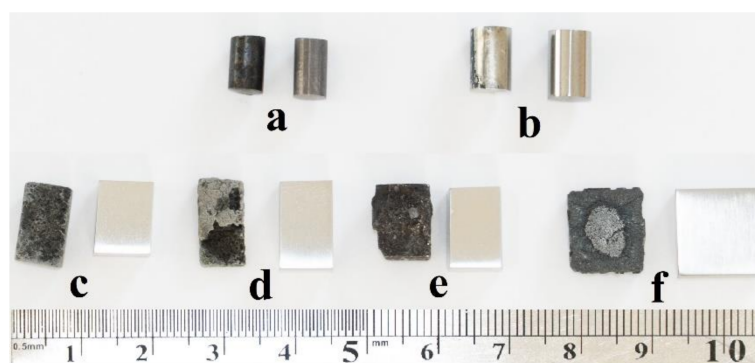


Figure 2. Appearance of metals and alloys before and after contacting with Bi-Li alloy at 650 °C for 100 h: tantalum (a); molybdenum (b); VDM® Alloy C-4 (c); KhN62M (d); VDM® Alloy 59 (e); and Hastelloy® G-35® (f).

Samples of metallic tantalum and molybdenum after the corrosion tests were separated from the Bi-Li alloy, washed, and their weight loss determined. The concentration of molybdenum and tantalum in the Bi-Li alloy samples was determined by ICP-AES and XRF analysis (Table 3). The results obtained by these two methods showed satisfactory agreement. Moreover, experimentally measured concentrations of tantalum and molybdenum in Bi-Li alloys correlated well with the literature data on solubility of Ta and Mo in liquid bismuth. Solubility of molybdenum in liquid bismuth does not exceed 10^{-4} wt.% at 1030 °C [23], and tantalum content in liquid bismuth after 120 h of contact at 778 °C was reported below 10^{-5} wt.% [24].

Table 3. Content of corrosion products in Bi-Li alloys held in contact with tantalum or molybdenum at 650 °C for 100 h.

System	Element	Element Content (wt.%)	
		XRF	ICP-AES
(Bi-Li)-Ta	Ta	0.0016 ± 0.0001	0.0017 ± 0.0001
(Bi-Li)-Mo	Mo	0.0011 ± 0.0001	0.0010 ± 0.0001

The weight loss of metallic samples was used to calculate the corrosion rates in Bi-Li alloys (gravimetric method). Additionally, the corrosion rates of metals were calculated from the content of corrosion products in the metallic alloy (analytical method). The results are summarized in Table 4.

Table 4. Corrosion rates of molybdenum and tantalum in liquid Bi-Li (5 mol.%) alloys determined by various methods after 100 h contact at 650 °C.

System	Corrosion Rate (mm/year) According to		
	Sample's Weight Loss	XRF Analysis	ICP-AES Analysis
Ta in (Bi-Li)	0.022 ± 0.003	0.092 ± 0.006	0.098 ± 0.005
Mo in (Bi-Li)	0.013 ± 0.002	0.071 ± 0.006	0.068 ± 0.005

The corrosion rates determined by the gravimetric method were several times lower than the corrosion rates calculated from the analysis of molybdenum and tantalum content in Bi-Li alloys. This discrepancy was caused by adhesion of bismuth to the surface of metals; the residual amounts of bismuth did not allow correctly determining the weight loss of the samples by the gravimetric method. Such behavior is very common and was noted in previous corrosion studies performed in liquid bismuth [27–35]. As a result, on several occasions, gravimetric analysis was rejected for determining corrosion rates of materials in liquid bismuth [27,28]. However, more often, various methods have been employed for

removing remaining bismuth from sample surfaces, and these include holding the samples in silicone [29,30], glycerol [31,32] or hot oil [33] at 150–180 °C; evaporating bismuth at elevated temperatures [25]; and treating samples in acidic solutions [29,34,35]. In the present study, to remove bismuth, the samples after the experiments were kept in dilute nitric acid to dissolve the bismuth. After the etching process, the solutions were analyzed to determine the content of molybdenum and tantalum and ensure that there was no loss of Mo and Ta during this procedure. The corrosion rates as calculated from the sample weight loss after removing traces of bismuth were ca. 0.07 mm/year for molybdenum and ca. 0.09 mm/year for tantalum and agreed very well with the values obtained by other techniques (Table 4).

After contact with liquid BLA, samples of molybdenum and tantalum were examined by SEM to determine possible nature of the metals' surface degradation (Figure 3). The results revealed no significant changes in the microstructure of metals; the surface was uniform with no significant damage. The bulk of the metals showed typical single-phase microstructure. The microstructure of the surface layer of the samples did not differ from the bulk. SEM–EDS analysis of the surface of molybdenum and tantalum samples showed that the elemental composition of the surface layer remained unchanged (Figure 4). No oxygen-containing phases—that can be formed if there was oxygen contamination in the atmosphere of the experimental cell—were detected on the surface. Lithium does not form intermetallic compounds with molybdenum or tantalum, and the solubility of these metals in lithium does not exceed 10^{-4} wt.% at 1000 °C [36–38].

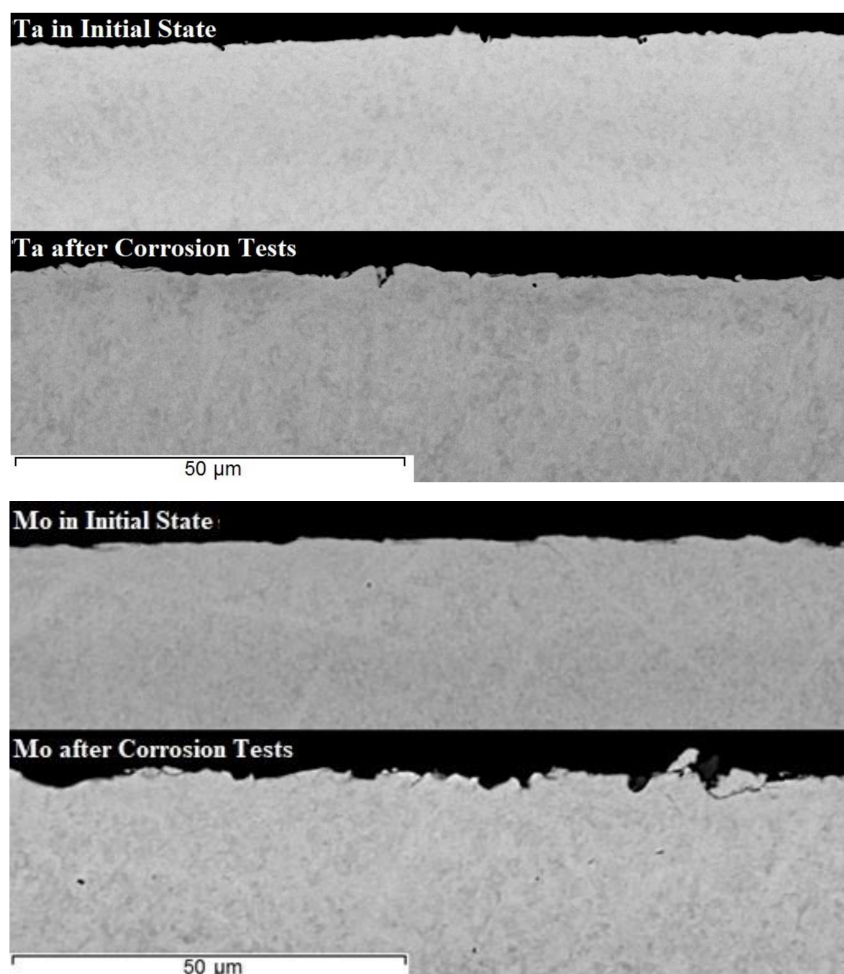


Figure 3. BSE-SEM images of the surface of molybdenum and tantalum samples before and after contacting Bi–Li (5 mol.%) alloy at 650 °C for 100 h.

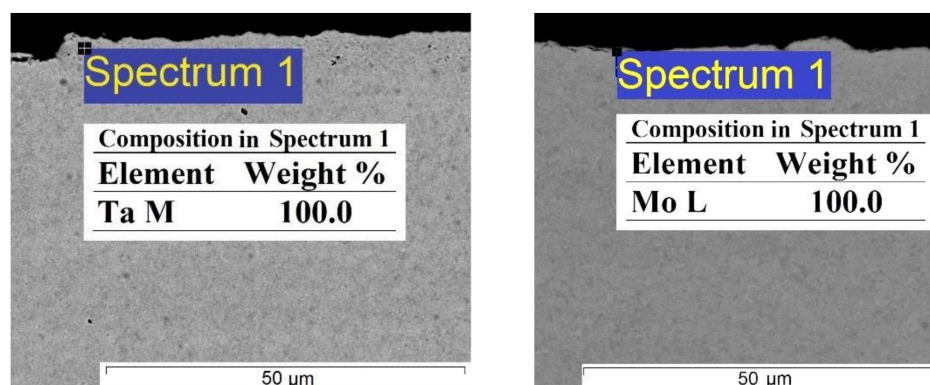


Figure 4. Composition of the surface layer of tantalum and molybdenum samples after 100 h contact with Bi–Li (5 mol.%) alloy at 650 °C.

The high purity of the BLA, molybdenum, and tantalum allowed excluding the possible chemical interaction of impurities with Mo and Ta. The major impurity in bismuth is silver (0.0012 wt.%), which does not form intermetallic compounds with tantalum or molybdenum [39–41] and, therefore, cannot influence the process of dissolution of these metals in Bi–Li alloys. Thus, the composition of BLA after the corrosion tests and the sample surface allow concluding that the corrosion rates of molybdenum and tantalum are determined by dissolution of these metals in bismuth. Such a conclusion is supported by the literature data [22–24,27].

The corrosion rates of nickel alloys could not be estimated using the gravimetric method since a significant amount of bismuth remained on the surface and in the bulk of the alloy samples. The microstructure of nickel alloys before and after the corrosion tests is shown in Figure 5. Interaction with BLA resulted in significant changes in nickel alloy microstructure. Prior to the corrosion tests, the alloys exhibited a solid solution single-phase structure. After the corrosion tests different phases appeared in the bulk on the samples (Figure 5). On first glance, these phases can be considered as the signs of corrosion destruction or pitting. However, a more detailed investigation showed that these pitting marks were in fact separate phases formed as a result of the interaction of alloys with BLA. Examining the samples in the back-scattered electron (BSE) regime revealed “dark”, “gray”, and “light” phases. Examples of microstructure of alloys with minimal and maximal nickel content, i.e., VDM® Alloy C-4 (67.4 wt.% Ni) and Hastelloy® G-35® (57.2 wt.% Ni), are shown in Figure 6.

SEM–EDS analysis of the phases formed in the alloys showed that “dark” phases consisted mostly of chromium, “gray” phases consisted mostly of molybdenum, and “light” phases of bismuth (Figure 7). Therefore, it can be concluded that nickel was almost completely etched from the bulk of the samples due to high solubility of nickel in bismuth (~7 wt.% at 650 °C [23]) and diffused into the liquid phase. This mechanism was confirmed by the results of chemical analysis of BLA after the experiments (Table 5). In addition to nickel, small concentrations of other alloy components, i.e., Cr, Mo, and Fe, were detected in Bi–Li alloy. No individual phases of Bi–Ni intermetallics were detected on the photographs. EDS analysis of various regions showed non-uniformity of the composition of the bismuth–nickel alloy formed during dissolution and following crystallization of the studied alloys. Intermetallic compounds of bismuth and nickel (Table 1) were not formed due to high solubility of nickel in liquid bismuth. Under the conditions of the experiments, the amount of solvent (bismuth) was so large that the formation of intermetallic compounds was suppressed by the dissolution process. It was shown, for example, that BiNi and Bi₃Ni phases were unstable in the presence of excess liquid bismuth and dissolved until bismuth was saturated with nickel [35].

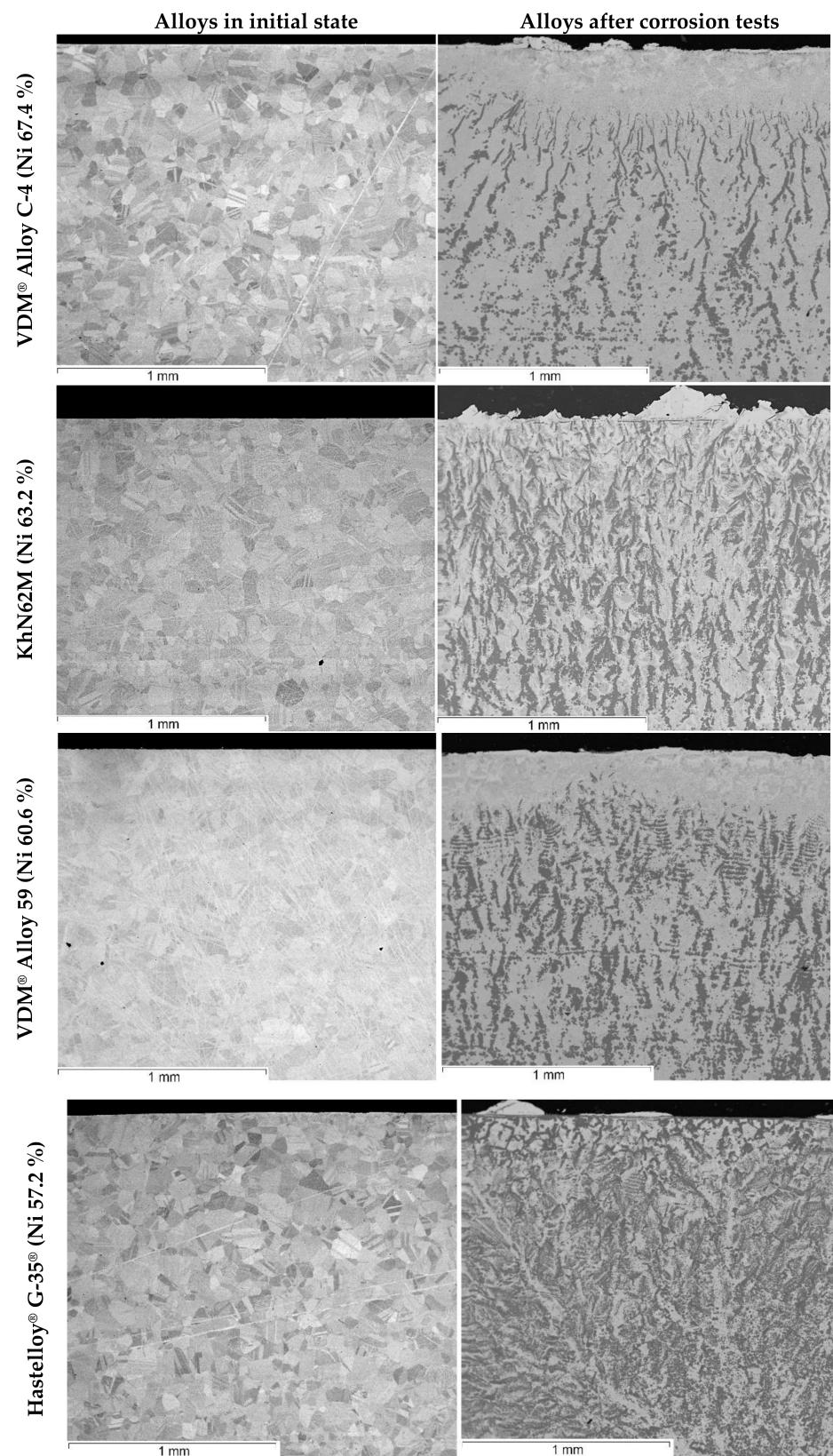


Figure 5. BSE-SEM images of microstructure of alloy samples before and after contacting BLA at 650 °C for 100 h.

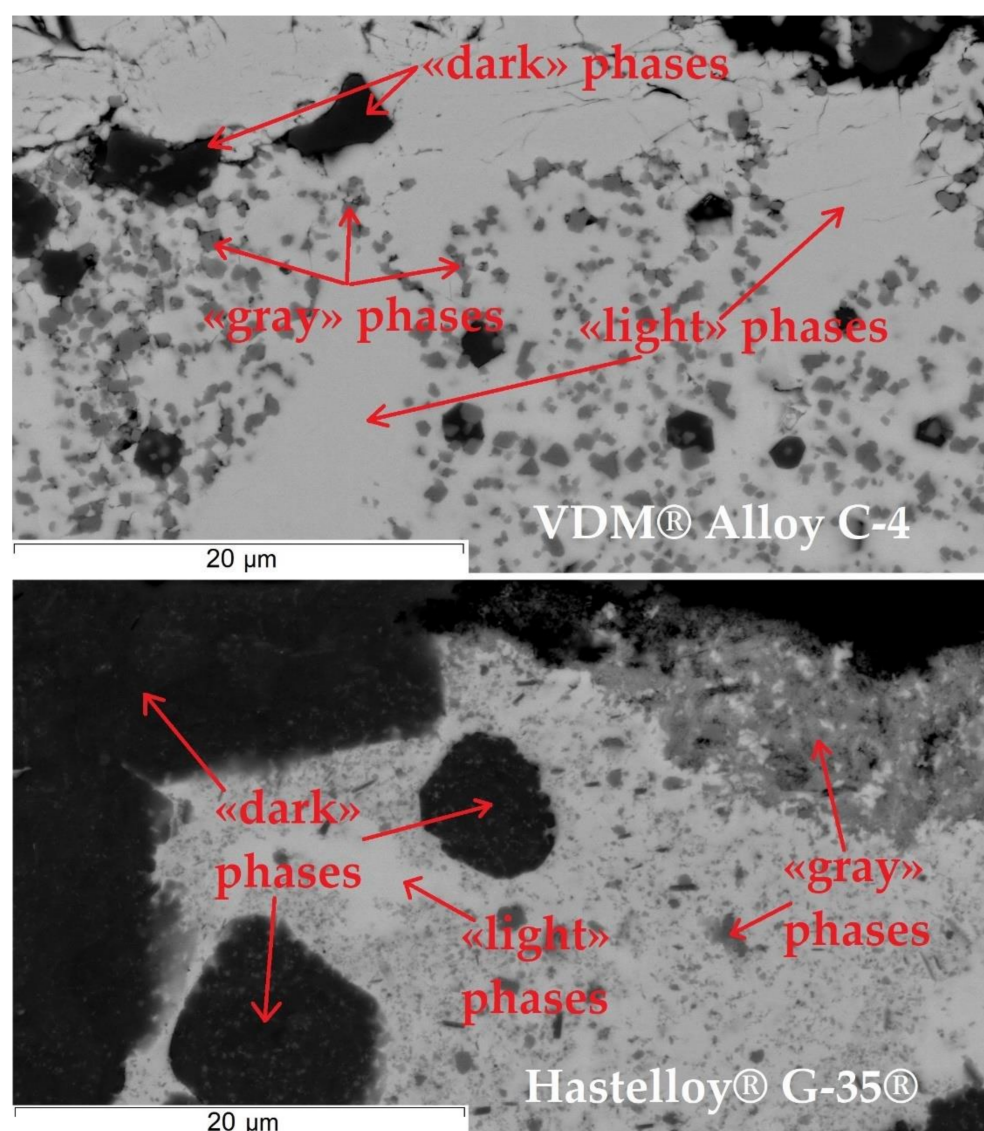


Figure 6. BSE-SEM images of new phases in nickel-based alloys after 100 h contact with BLA at 650 °C.

Table 5. Content of corrosion products in Bi–Li alloys held in contact with Ni-based alloys at 650 °C for 100 h, wt.%.

Alloys	Corrosion Product Content (wt. %) Determined by						
	XRF			ICP–AES			
	Ni	Cr	Mo	Ni	Cr	Mo	Fe
Hastelloy® G-35®	0.83	0.001	<0.001	0.95	0.0002	0.0001	<0.001
KhN62M	0.77	<0.001	<0.001	0.86	0.0001	0.0001	<0.001
VDM® Alloy C-4	1.02	<0.001	<0.001	1.12	0.0002	0.0002	<0.001
VDM® Alloy 59	1.04	<0.001	<0.001	1.21	0.0002	0.0001	<0.001

Formation of “dark” and “gray” phases can be explained in the following way. Solubility of chromium and molybdenum in the BLA is very low [22,23]. At the temperature of the experiments, Cr and Mo predominantly remained in the solid state and formed particles of a solid solution (“dark” and “gray” phases). Since the corrosion tests were carried out under static conditions, these particles retained the core of the samples for a long time. Upon cooling, Bi–Li alloy with dissolved nickel crystallized. Solid (Cr, Mo)

particles acted as the centers of crystallization. As a result of these processes, a characteristic structure of the ingot, shown in Figures 5 and 6, was formed. There are no previous studies of corrosion of nickel alloys in liquid bismuth or BLA. Corrosion of austenitic steels in bismuth and lead–bismuth eutectic (LBE) resulted in transformation of the austenitic phase into ferritic due to the predominant dissolution of nickel [28,31,42]. The surface of steel samples became porous, and the pores were filled by liquid metals. Similar behavior was observed in the previous work; however, the processes taking place were intensified due to high nickel content in the studied materials.

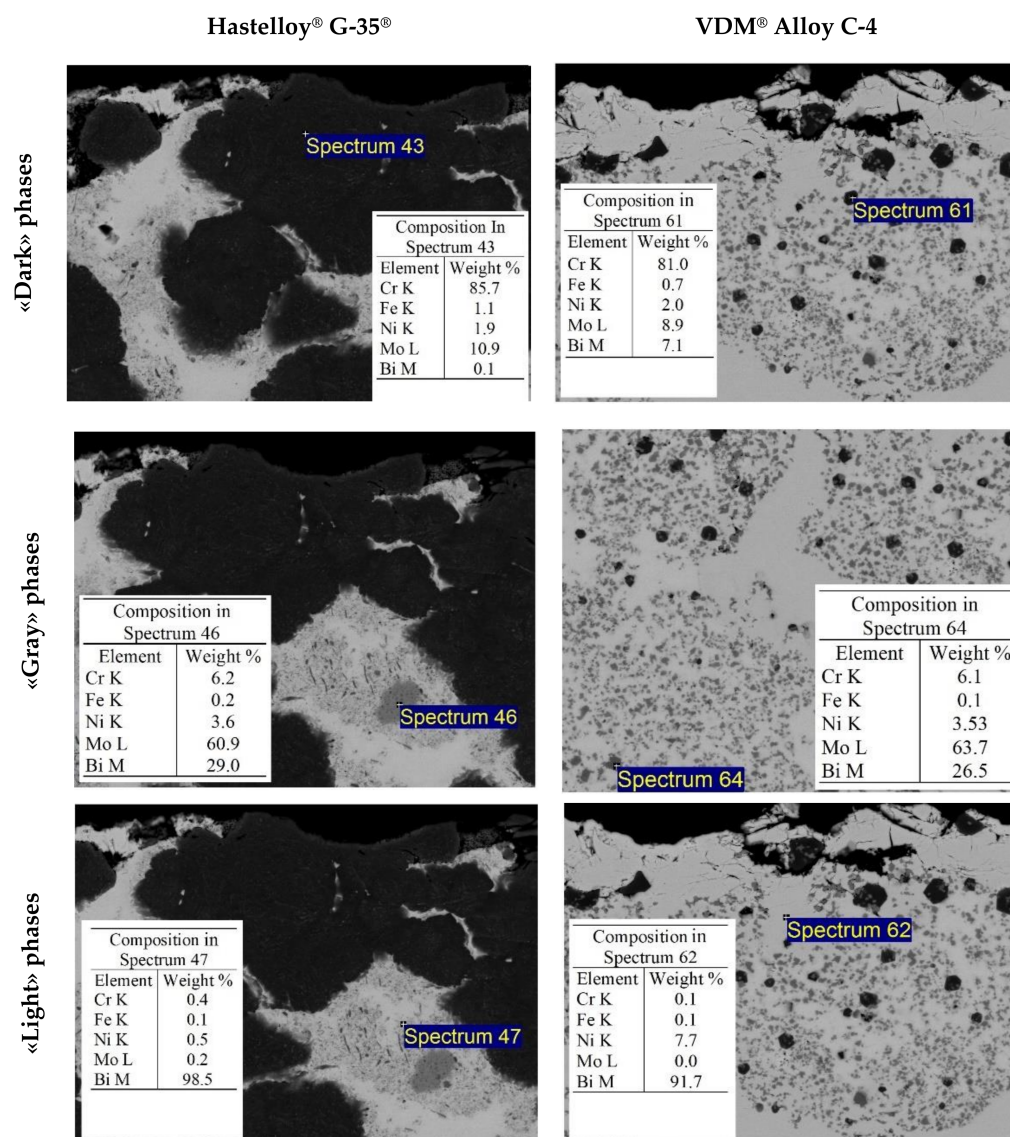


Figure 7. Composition of phases formed in nickel-based alloys after 100 h contact with Bi–Li alloys (5 mol.%) at 650 °C.

Therefore, the corrosion rates of nickel-based alloys were determined using the results of chemical analysis of Bi–Li alloys after the corrosion tests. The obtained values are listed in Table 6. It is clear that nickel-based alloys underwent significant corrosion destruction and showed unacceptably high corrosion rates (exceeding the corrosion rates of individual Mo and Ta more than 400 times).

Table 6. Corrosion rate of samples of metallic materials after 100 h in contact with liquid Bi–Li (5 mol.%) at 650 °C (mm/year).

Alloy	Corrosion Rate (mm/year) According to	
	XRF	ICP–AES
Hastelloy® G-35®	27	32
KhN62M	30	34
VDM® Alloy 59	30	36
VDM® Alloy C-4	32	35

4. Conclusions

The corrosion behavior of several metallic materials in contact with a liquid Bi–Li (5 mol.%) alloy was studied. The experiments were carried out under identical conditions for all samples (650 °C, 100 h). Several experimental methods (SEM/EDS, XRF, and ICP–AES) were used to determine the mechanisms of interaction of materials with molten Bi–Li.

It was confirmed that physical dissolution of metal samples in liquid metals was the main mechanism of corrosion. Due to the low values of solubility for molybdenum and tantalum in liquid bismuth, these metals did not significantly corrode in the liquid alloy. The corrosion rates were ca. 0.07 mm/year for molybdenum and ca. 0.09 mm/year for tantalum. The surface of the samples of these metals showed uniform corrosion.

Nickel-based alloys underwent significant structural changes after contact with Bi–Li alloys, which resulted primarily from a high solubility of nickel in liquid bismuth. Bismuth selectively leached nickel from the alloys. Molybdenum and chromium (principal alloying elements in the alloys) did not dissolve in bismuth and formed separate phases enriched in chromium and molybdenum. Dissolution of nickel resulted in the formation of pores that were filled by bismuth that formed a multiphase structure of a new bismuth-based alloy. Samples of nickel alloys underwent considerable degradation, and these alloys cannot therefore be used as construction materials working in contact with bismuth-containing liquid media. Moreover, when designing a process for extraction of elements from SNF to liquid bismuth, it must be ensured that there is no bismuth in the technological streams that may contact units made of nickel alloys, to avoid serious corrosion issues and degradation of nickel-based materials.

Author Contributions: Conceptualization, I.B.P. and V.A.V.; Methodology, A.V.A.; Software, A.Y.Z.; Validation, R.R.A. and A.V.A.; Formal Analysis, A.Y.Z. and A.V.A.; Investigation, R.R.A. and A.I.T.; Resources, I.B.P.; Data Curation, I.B.P.; Writing—Original Draft Preparation, A.V.A.; Writing—Review and Editing, I.B.P. and V.A.V.; Visualization, S.V.B.; Supervision, I.B.P.; Project Administration, I.B.P. and S.V.B.; Funding Acquisition, I.B.P. All authors have read and agreed to the published version of the manuscript.

Funding: This study was financially supported by the JSC “Science and Innovations” and JSC RIAR.

Institutional Review Board Statement: Not applicable.

Informed Consent Statement: Not applicable.

Data Availability Statement: The data presented in this study are available on request from the corresponding author.

Conflicts of Interest: The authors declare no conflict of interest.

References

1. International Atomic Energy Agency. *Liquid Metal Cooled Reactors: Experience in Design and Operation*; IAEA-TECDOC-CD-1569; IAEA: Vienna, Austria, 2008.
2. Subbotin, V.I.; Arnol'dov, M.N.; Kozlov, F.A.; Shimkevich, A.L. Liquid-Metal Coolants for Nuclear Power. *At. Energy* **2002**, *92*, 29–40. [[CrossRef](#)]
3. Zrodnikov, A.V.; Gromov, B.F.; Grigoryev, O.G.; Dedoul, A.V.; Toshinsky, G.I.; Dragunov, Y.G.; Stepanov, V.S. Use of Russian technology of ship reactors with lead-bismuth coolant in nuclear power (IAEA-TECDOC-1172). *IAEA* **2000**, *31*, 127–155.

4. Zhang, X.D.; Liu, J. Perspective on liquid metal enabled space science and technology. *Sci. China Technol. Sci.* **2020**, *63*, 1127–1140. [\[CrossRef\]](#)
5. International Atomic Energy Agency. *Spent Fuel Reprocessing Options*; IAEA-TECDOC-CD-1587; IAEA: Vienna, Austria, 2009.
6. Weisenburger, A.; Lang, F.; Müller, G. Material and experimental issues related to the use of liquid metals as heat transfer media for CSP tower receivers. *AIP Conf. Proc.* **2018**, *2033*, 080005.
7. Zhuk, N.P. *Corrosion and Metal Protection Theory Course*; Alyans: Moscow, Russia, 2006.
8. Borishansky, V.M. *Liquid metal coolants*; Atomizdat: Moscow, Russia, 1967.
9. Shrier, L.L.; Jarman, R.A.; Burstein, G.T. Mechanisms of Liquid metal Corrosion. In *Corrosion (Metal/Environment Reactions)*, 3rd ed.; Reed Educational and Professional Publishing Ltd.: Butterworth-Heinemann Linacn House, Jordan Hill, Oxford, UK, 1994; Volume 1, pp. 464–465.
10. Tsuprun, L.I.; Tarytina, M.I. *Metallurgy of Nuclear Energy*; Gostekhizdat: Moscow, Russia, 1956.
11. Joseph, B.; Picat, M.; Barbier, F. Liquid metal embrittlement: A state-of-the-art appraisal. *Eur. Phys. J. Appl. Phys.* **1999**, *5*, 19–31. [\[CrossRef\]](#)
12. Pereiro-López, E.; Ludwig, W.; Bellet, D. Discontinuous penetration of liquid Ga into grain boundaries of Al polycrystals. *Acta Mater.* **2004**, *52*, 321–332. [\[CrossRef\]](#)
13. Pereiro-López, E.; Ludwig, W.; Bellet, D.; Lemaignan, C. In situ investigation of Al bicrystal embrittlement by liquid Ga using synchrotron imaging. *Acta Mater.* **2006**, *54*, 4307–4316. [\[CrossRef\]](#)
14. Sigle, W.; Richter, G.; Ruhle, M.; Schmidt, S. Insight into the atomic-scale mechanism of liquid metal embrittlement. *Appl. Phys. Lett.* **2006**, *89*, 121911. [\[CrossRef\]](#)
15. Asl, K.M.; Luo, J. Impurity effects on the intergranular liquid bismuth penetration in polycrystalline nickel. *Acta Mater.* **2012**, *60*, 149–165. [\[CrossRef\]](#)
16. James, J.A.; Trotman, J. Corrosion of steels in liquid bismuth and lead. *J. Iron Steel Inst.* **1960**, *194*, 319–323.
17. Horsley, G.W.; Maskrey, J.T. The corrosion of 2.25Cr–1Mo steel by liquid bismuth. *J. Iron Steel Inst.* **1958**, *189*, 139–148.
18. Dawe, D.W.; Parry, G.W.; Wilson, G.W. Study of compatibility of some creep resistant steels with liquid bismuth in non-isothermal systems. *J. Br. Nucl. Energy Conf.* **1960**, *5*, 24–29.
19. Stephan, H.R.; Koshuba, W.J. *Circulation of Bismuth at Elevated Temperatures, Progress Report on Project 2-01*; NEPA-1675; NEPA Division Fairchild Engine and Airplane Corporation: New York, NY, USA, 1950.
20. Polovov, I.B.; Abramov, A.V.; Alimgulov, R.R.; Zolotarev, D.A.; Trubcheninova, A.I.; Gibadullina, A.F.; Volkovich, V.A.; Zhilyakov, A.Y.; Khotinov, V.A.; Belikov, S.V. Corrosion of Metallic Materials in Molten FLiNaK. *ECS Trans.* **2020**, *98*, 453–462. [\[CrossRef\]](#)
21. Balandin, Y.F.; Markov, V.G. *Structural Materials for Installations with Liquid Metal Heat Carriers*; Sudpromgiz: Leningrad, Russia, 1961.
22. Okamoto, H.; Schlesinger, M.E.; Mueller, E.M. (Eds.) Bi (Bismuth) Binary Alloy Phase Diagrams, Alloy Phase Diagrams. In *ASM Handbook*; ASM International: Materials Park, OH, USA, 2016; Volume 3, pp. 201–217.
23. Lyakisheva, N.P. (Ed.) *State Diagrams of Double Metal Systems: Handbook*; Elsevier Ltd.: Amsterdam, The Netherlands, 1996; Volume 1.
24. Garg, S.P.; Krishnamurthy, N. The Bi-Ta (bismuth-tantalum) system. *JPE* **1992**, *13*, 269–270. [\[CrossRef\]](#)
25. Dybkov, V.I.; Barmak, K.; Lengauer, W.; Gas, P. Interfacial interaction of solid nickel with liquid bismuth and Bi-base alloys. *J. Alloys Compd.* **2005**, *389*, 61–74. [\[CrossRef\]](#)
26. Polovov, I.B.; Abramov, A.V.; Gibadullina, A.F.; Alimgulov, R.R.; Karpov, V.V.; Zhilyakov, A.Y.; Khotinov, V.A. The effect of microstructure on the corrosion resistance of VDM® alloy C-4 in molten salts. *J. Alloys Compd.* **2019**, *810*, 151758. [\[CrossRef\]](#)
27. Reed, E.L. Stability of Refractories in Liquid Metals. *J. Am. Ceram. Soc.* **1954**, *37*, 146–152. [\[CrossRef\]](#)
28. Yamaki, E.; Ginestar, K.; Martinelli, L. Dissolution mechanism of 316L in lead–bismuth eutectic at 500°C. *Corros. Sci.* **2011**, *53*, 3075–3085. [\[CrossRef\]](#)
29. Martín-Muñoz, F.J.; Soler-Crespo, L.; Gómez-Briceño, D. Corrosion behaviour of martensitic and austenitic steels in flowing lead–bismuth eutectic. *J. Nucl. Mater.* **2011**, *416*, 87–93. [\[CrossRef\]](#)
30. Kurata, Y.; Sato, H.; Yokota, H.; Suzuki, T. Applicability of Al-Powder-Alloy Coating to Corrosion Barriers of 316SS in Liquid Lead-Bismuth Eutectic. *Jpn. Inst. Metals. Mater. Trans.* **2011**, *52*, 1033–1040. [\[CrossRef\]](#)
31. Barbier, F.; Rusanov, A. Corrosion behavior of steels in flowing lead–bismuth. *J. Nucl. Mater.* **2001**, *296*, 231–236. [\[CrossRef\]](#)
32. Kurata, Y.; Saito, S. Temperature Dependence of Corrosion of Ferritic/Martensitic and Austenitic Steels in Liquid Lead-Bismuth Eutectic. *Jpn. Inst. Metals. Mater. Trans.* **2009**, *50*, 2410–2417. [\[CrossRef\]](#)
33. Mueller, G.; Schumacher, G.; Weisenburger, A.; Heinzl, A.; Zimmermann, F.; Tomohiro, F.; Kazumi, A. *Study on Pb/Bi Corrosion of Structural and Fuel Cladding Materials for Nuclear Applications*; ASM International: Materials Park, OH, USA, 2004.
34. Dörmstedt, P.; Lundberg, M.; Szakalos, P. Corrosion Studies of Low-Alloyed FeCrAl Steels in Liquid Lead at 750 °C. *Oxid. Met.* **2019**, *91*, 511–524. [\[CrossRef\]](#)
35. Das, C.; Kishore, R.; Fotedar, R. Corrosion Compatibility Studies of Stainless Steel 304L in Flowing Liquid Lead Bismuth Eutectic. *Trans. Indian Inst. Met.* **2011**, *64*, 417–423. [\[CrossRef\]](#)
36. Garg, S.P.; Venkatraman, M.; Krishnamurthy, N. *Binary Alloy Phase Diagrams*, 2nd ed.; Massalski, T.B., Ed.; Materials Information Society: Materials Park, OH, USA, 1990; Volume 3.

-
37. Subramanian, P.R. Li-Mo (Lithium-Molybdenum). In *Binary Alloy Phase Diagrams*, 2nd ed.; Massalski, T.B., Ed.; ASM International: Materials Park, OH, USA, 1990; Volume 3, pp. 2446–2447.
 38. Gryaznov, G.M.; Evtikhin, V.A.; Lyublinsky, I.E. *Materials Science of Liquid Metal Systems of Thermonuclear Reactors*; Energoatomizdat: Moscow, Russia, 1989.
 39. Kieffer, R.; Windisch, S.; Nowotny, H. Niobium–Tantalum Infiltrated Alloys. *Metall* **1963**, *17*, 669–677.
 40. Brewer, L.; Lamoreaux, R.H. *Molybdenum, Physico-chemical Properties of its Compounds and Alloys*; Atomic Energy Review; Special Issue No.7; IAEA: Vienna, Austria, 1980.
 41. Baren, M.R. The Ag-Mo (silver-molybdenum) system. *Bull. Alloy Phase Diagr.* **1990**, *11*, 548–549. [[CrossRef](#)]
 42. Simon, N.; Terlain, A.; Flament, T. The compatibility of austenitic materials with liquid Pb–17Li. *Corros. Sci.* **2001**, *43*, 1041–1052. [[CrossRef](#)]